

# Particle Identification Using Boosted Decision Trees in the Semi-Digital Hadronic Calorimeter Prototype

---

## The CALICE Collaboration

**D. Boumediene,**

*Université Clermont Auvergne, Université Blaise Pascal, CNRS/IN2P3, LPC, 4 Av. Blaise Pascal, TSA/CS 60026, F-63178 Aubière, France*

**A. Pingault, M. Tytgat**

*Ghent University, Department of Physics and Astronomy, Proeftuinstraat 86, B-9000 Gent, Belgium*

**B. Bilki, D. Northacker, Y. Onel**

*University of Iowa, Dept. of Physics and Astronomy, 203 Van Allen Hall, Iowa City, IA 52242-1479, USA*

**G. Cho, D-W. Kim, S. C. Lee, W. Park, S. Vallecorsa**

*Gangneung-Wonju National University Gangneung 25457, South Korea*

**Y. Deguchi, K. Kawagoe, Y. Miura, R. Mori, I. Sekiya, T. Suehara, T. Yoshioka**

*Department of Physics and Research Center for Advanced Particle Physics, Kyushu University, 744 Motoooka, Nishi-ku, Fukuoka 819-0395, Japan*

**L. Caponetto, C. Combaret, R. Ete\*, G. Garillot, G. Grenier, J-C. Ianigro, T. Kurca, I. Laktineh, B. Liu<sup>a</sup>, B. Li, N. Lumb, H. Mathez, L. Mirabito, A. Steen<sup>†</sup>**

*Univ Lyon, Univ CLaude Bernard Lyon 1, CNRS/IN2P3, IP2I Lyon, F-69622 Villeurbanne, France*

**E. Calvo Alamillo, M.C. Fouz, J. Marin, J. Navarrete, J. Puerta Pelayo, A. Verdugo**

*CIEMAT, Centro de Investigaciones Energeticas, Medioambientales y Tecnologicas, Madrid, Spain*

**F. Corriveau, B. Freund<sup>‡</sup>**

*Department of Physics, McGill University, Ernest Rutherford Physics Bldg., 3600 University Ave., Montréal, Québec, Canada H3A 2T8*

**M. Chadeeva, M. Danilov<sup>§</sup>**

*P. N. Lebedev Physical Institute of the Russian Academy of Sciences, 53 Leninsky  
prospekt, Moscow, 119991 Russia*

**L. Emberger, C. Graf, F. Simon, C. Winter**

*Max-Planck-Institut für Physik, Föhringer Ring 6, D-80805 Munich, Germany*

**J. Bonis, D. Breton, P. Cornebise, A. Gallas, J. Jeglot, A. Irles, J. Maalmi,  
R. Pöschl, A. Thiebault, F. Richard, D. Zerwas**

*Université Paris-Saclay, CNRS/IN2P3, IJCLab, 91405 Orsay, France*

**M. Anduze, V. Balagura, V. Boudry, J-C. Brient, E. Edy, F. Gastaldi,  
R. Guillaumat, F. Magniette, J. Nanni, H. Videau**

*Laboratoire Leprince-Ringuet (LLR) – CNRS, École polytechnique, Institut  
Polytechnique de Paris Palaiseau, F-91128 France*

**S. Callier, F. Dulucq, Ch. de la Taille, G. Martin-Chassard, L. Raux,  
N. Seguin-Moreau**

*Laboratoire OMEGA – École Polytechnique-CNRS/IN2P3, Palaiseau, F-91128 France*

**J. Cvach, M. Janata, M. Kovalcuk, J. Kvasnicka, I. Polak, J. Smolik, V. Vrba,  
J. Zalesak, J. Zuklin**

*Institute of Physics, The Czech Academy of Sciences, Na Slovance 2, CZ-18221 Prague 8,  
Czech Republic*

**Y.Y. Duan, S. Li, J. Guo, J.F. Hu, F. Lagarde, B. Liu<sup>a</sup>, Q.P. Shen, X. Wang,  
W.H. Wu, H.J. Yang, Y.F. Zhu**

*Tsung-Dao Lee Institute, Institute of Nuclear and Particle Physics, School of Physics and  
Astronomy, Shanghai Jiao Tong University, Key Laboratory for Particle Physics,  
Astrophysics and Cosmology (Ministry of Education), Shanghai Key Laboratory for  
Particle Physics and Cosmology, 800 Dongchuan Road, Shanghai, 200240, P. R. China*

<sup>a</sup> *Corresponding author*

*E-mail: b.Liu@ipnl.in2p3.fr, 610412075@sjtu.edu.cn*

**ABSTRACT:** The CALICE Semi-Digital Hadronic CALorimeter (SDHCAL) prototype using Glass Resistive Plate Chambers as a sensitive medium is the first technological prototype of a family of high-granularity calorimeters developed by the CALICE collaboration to equip the experiments of future leptonic colliders. It was exposed to beams of hadrons, electrons and muons several times in the CERN PS and SPS beamlines between 2012 and 2018. We present here a new method of particle identification within the SDHCAL using the Boosted Decision Trees (BDT) method applied to the data collected in 2015. The performance of the method is tested first with Geant4-based simulated events and then on the data collected by the SDHCAL in the energy range between 10 and 80 GeV with 10 GeV energy steps. The BDT method is then used to reject the electrons and muons that contaminate the SPS hadron beams.

KEYWORDS: Calorimeters, MVA.

---

\*Now at DESY

†Now at NTU

‡Also at Argonne National Laboratory

§Also at MIT

---

## Contents

<b>1. Introduction</b>	<b>1</b>
<b>2. Monte Carlo samples and beam data samples</b>	<b>2</b>
<b>3. Particle identification using Boosted Decision Trees</b>	<b>3</b>
3.1 BDT input variables	3
3.2 The two approaches to build the BDT-based classifier	5
3.2.1 MC Training Approach	5
3.2.2 Data Training Approach	10
<b>4. Results</b>	<b>11</b>
<b>5. Conclusion</b>	<b>13</b>
<b>6. Acknowledgements</b>	<b>14</b>

---

## 1. Introduction

The Semi-Digital Hadronic CALorimeter (SDHCAL) [1] is the first of a series of technological high-granularity prototypes developed by the CALICE collaboration. These technological prototypes have their readout electronics embedded in the detector and they are power-pulsed to reduce the power consumption in experiments proposed within the International Linear Collider (ILC) project [2]. The mechanical structure of these prototypes is part of their absorber. All these aspects increase the compactness of the calorimeters and improve their suitability to apply the Particle Flow Algorithm (PFA) techniques [3, 4, 5]. The SDHCAL is made of 48 active layers, each of them equipped with a  $1\text{ m} \times 1\text{ m}$  Glass Resistive Plate Chamber (GRPC) and an Active Sensor Unit (ASU) of the same size hosting on one face (the one in contact with the GRPC) pickup pads of  $1\text{ cm} \times 1\text{ cm}$  and 144 HARDROC2 ASICs [6] on the the other face. The GRPC and the ASU are assembled within a cassette made of two stainless steel plates, 2.5 mm thick each. The 48 cassettes are inserted in a self-supporting mechanical structure made of 51 plates, 15 mm thick each, of the same material as the cassettes, bringing the total absorber thickness to 20 mm per layer. The empty space between two consecutive plates is 13 mm to allow the insertion of one cassette of 11 mm thickness. The HARDROC2 ASIC has 64 channels to read out

18 64 pickup pads. Each channel has three parallel digital circuits whose parameters can be  
19 configured to provide 2-bit encoded information indicating if the charge seen by each pad  
20 has passed any of the three different thresholds associated to each digital circuit. This  
21 multi-threshold readout is proposed to improve on the energy reconstruction of hadronic  
22 showers at high energy ( $> 30$  GeV) with respect to the simple binary readout mode as  
23 explained in Ref. [7].

24 The SDHCAL was exposed several times to different kinds of particle beams in the  
25 CERN PS and SPS beamlines between 2012 and 2018. The energy reconstruction of  
26 hadronic showers within the SDHCAL using the associated number of fired pads with  
27 multi-threshold readout information is presented in Ref. [7]. The contamination of the  
28 SPS hadron beams such as electrons and muons and the absence of Cherenkov counters  
29 during the data taking require the use of the event topology to select the hadronic events  
30 before reconstructing their energy. Although the rejection of muons based on the average  
31 number of hits per crossed layer is efficient, the rejection of electrons is more difficult  
32 because some hadronic showers behave in similar way as the electromagnetic ones in  
33 particular at low energy. To reject the electron events, the analysis presented in Ref. [7]  
34 requires the shower to start after the fifth layer. Almost all of the electrons are expected to  
35 start showering before crossing the equivalent of 6 radiation lengths ( $X_0$ )<sup>1</sup>. Although this  
36 selection is found to have no impact on the hadronic energy reconstruction, it represents  
37 0.6 interaction length ( $\lambda_I$ ) and thus reduces the amount of the hadronic showers available  
38 for analysis.

39 In this paper we explore another method to reject the electron and muon contamina-  
40 tions, that is not based on the shower start requirement and does thus preserve the statistics.  
41 The new method is based on Boosted Decision Trees (BDT) [8, 9], a part of so-called Mu-  
42 tiVariate Analysis (TMVA) technique [10]. In the BDT, different variables associated to  
43 the topology of the event are exploited in order to distinguish between the hadronic and  
44 the electromagnetic showers, and also to identify muons including radiative ones that may  
45 exhibit a shower-like shape. In this paper, section 2 introduces the simulation and beam  
46 data samples which are used to study the performance of both the BDT and the standard  
47 method described in Ref. [7]. Section 3 describes the selected input variables of BDT and  
48 the two approaches to build the classifier of BDT. Section 4 presents the results of the  
49 hadron selection using BDT. Finally, section 5 gives the conclusion.

## 50 **2. Monte Carlo samples and beam data samples**

51 The SDHCAL prototype was exposed to pions, muons and electrons in the SPS of CERN  
52 in October 2015. In order to avoid GRPC saturation problems at high particle rate, only  
53 runs with a particle rate smaller than 1000 particles/spill are selected for the analysis. In  
54 these conditions, pion events at several energy points (10, 20, 30, 40, 50, 60, 70, 80 GeV)

---

<sup>1</sup>The longitudinal depth of the SDHCAL prototype layer is about  $1.2 X_0$ .

55 and muon events of 110 GeV were collected as well as electron events of 10, 15, 20,  
56 25, 30, 40, 50 GeV. While the electron and muon beams are rather pure, the pion beams  
57 are contaminated by two sources. One is the electron contamination despite the use of  
58 a lead filter to reduce the number of electrons. The other is the muon contamination  
59 resulting from pions decaying before reaching the prototype. To apply the BDT method,  
60 six variables are selected and used in the Toolkit for MultiVariate data Analysis (TMVA)  
61 package [10] to build the decision tree.

62 To study the performance of the BDT method, we use the Geant4.9.6 Toolkit pack-  
63 age [11] associated to the FTF-BIC<sup>2</sup> [12, 13] physics list to generate pion, electron and  
64 muon events under the same conditions as in the beam test at CERN-SPS beamline. For  
65 the training of the BDT, 10k events for each energy point from 10 GeV to 80 GeV with a  
66 step of 10 GeV for pions, muons and electrons were produced. The same amount of events  
67 of each species is produced and used to test the BDT method at the same time. Finally, the  
68 pure (> 99.5%) electron and muon data samples<sup>3</sup> are used as validation sets.

69 In order to render the particle identification independent of the energy of the different  
70 species and thus to extend the method applied here to a larger scope than the beam purifi-  
71 cation, the pion samples of different energies are mixed before using the BDT technique.  
72 The same procedure is applied for muon and electron samples.

### 73 **3. Particle identification using Boosted Decision Trees**

74 Thanks to the high granularity of the SDHCAL, we can use the MVA methods to mine  
75 the information of the shape of electromagnetic and hadronic shower to classify muons,  
76 electrons and pions. The BDT method is one of the widely used MVA methods to perform  
77 such classification tasks. The BDT is a model that combines many less selective decision  
78 trees<sup>4</sup> into a strong classifier to achieve a much better performance.

#### 79 **3.1 BDT input variables**

80 The six variables we use to distinguish hadronic showers from electromagnetic show-  
81 ers and from muons are described below. A common right-handed coordinate system is  
82 used throughout the SDHCAL whose 48 layers were placed perpendicular to the incoming  
83 beams. The origin of the system is defined as the center of the first of the 48 SDHCAL's  
84 layers. The  $x$ - $y$  plane is parallel to the SDHCAL layers and referred to as the transverse  
85 plane while the  $z$ -axis runs parallel to the incoming beam.

- 86 • **First layer of the shower (Begin)** : The probability of a particle to interact in the  
87 calorimeter depends on the particle nature and the calorimeter material properties.

---

<sup>2</sup>The FTF model is based on the Fritiof description of string excitation and fragmentation. The BIC model uses Geant4 binary cascade for primary protons and neutrons with energies below 10 GeV. It describes the production of secondary particles produced in interactions of protons and neutrons with nuclei.

<sup>3</sup>The purity of these samples is provided by the SPS electron and muon beams.

<sup>4</sup>A decision tree takes a set of input variables and splits input data recursively based on those variables.

88 The distribution of the coordinate  $z$  of the layer in which the first inelastic interaction  
 89 takes place, follows an exponential law. It is proportional to  $\exp(-\frac{z}{X_0})$  for electrons  
 90 and to  $\exp(-\frac{z}{\lambda_I})$  for pions, where  $X_0$  and  $\lambda_I$  are effective radiation length and nuclear  
 91 interaction length for the SDHCAL material composition, respectively. To define the  
 92 first layer in which the shower starts we look for the first layer along the incoming  
 93 particle direction, which contains at least 4 fired pads. To eliminate fake shower  
 94 starts due to accidental noise or a locally high multiplicity, the following 3 layers  
 95 after the first one are also required to have more than 4 fired pads in each of them.  
 96 Particles crossing the calorimeter without interaction are assigned the value of 48,  
 97 which is the case for most of the muons in the studied beam except the radiative  
 98 ones. Figure 1 shows the distribution of the first layer of the shower in the SDHCAL  
 99 prototype for pions, electrons and muons as obtained from the simulation and data.

- 100 • **Number of tracks segments in the shower (TrackMultiplicity):** Applying the  
 101 Hough Transform (HT) technique to single out the tracks in each event as described  
 102 in Ref. [14], we estimate the number of tracks segments in the pion, electron and  
 103 muon events. A HT-based segment candidate is considered as a track segment if  
 104 there are more than 6 aligned hits with not more than one layer separating two con-  
 105 secutive hits. Electron showers feature almost no track segment while most of the  
 106 hadronic showers have at least one. For muons, except for some radiative muons,  
 107 only one track is expected as can be seen in Fig. 2.
- 108 • **Ratio of shower layers over total hit layers (NinteractingLayers/NLayers):** This  
 109 is the ratio between the number of layers in which the Root Mean Square (RMS) of  
 110 the hits' position in the  $x$ - $y$  plane exceeds 5 cm in both  $x$  and  $y$  directions and the  
 111 total number of layers with at least one fired pad. It allows, as can be seen in Fig. 3,  
 112 an easy discrimination of muons (even the radiative ones) from pions and electrons.  
 113 It allows also a slight separation between pions and electrons.
- 114 • **Shower density (Density):** This is the average number of the neighbouring hits  
 115 located in the  $3 \times 3$  pads around one of the hits including the hit itself in the given  
 116 event. Figure 4 shows clearly that electromagnetic showers are more compact than  
 117 the hadronic showers as expected.
- 118 • **Shower radius (Radius):** This is the RMS of hits distance with respect to the event  
 119 axis. To estimate the event axis, the average positions of the hits in each of the ten  
 120 first fired layers of an event are used to fit a straight line. The straight line is then  
 121 used as the event axis. Figure 5 shows the average radius of the three particle species  
 122 in the SDHCAL.
- 123 • **Shower maximum position (Length):** This is the distance between the shower start  
 124 and the layer where the maximum RMS of hit transverse coordinates with respect

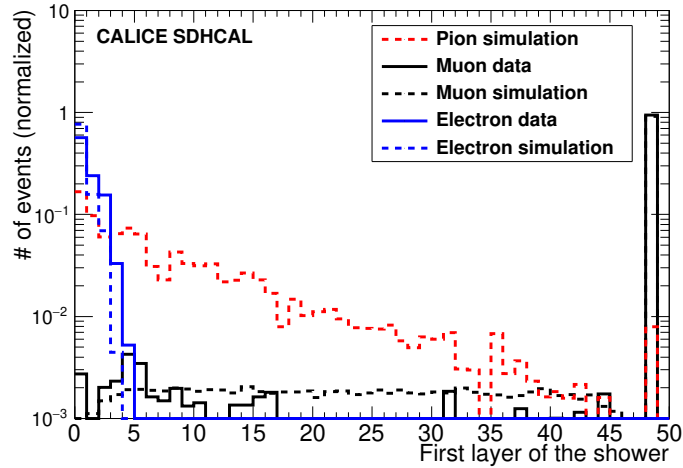


**Figure 1.** Distribution of the first layer of the shower (Begin). Layer 0 refers to the first layer of the prototype. Continuous lines refer to data while dashed ones to the simulation. Layer 48 is the virtual layer after the last layer and used to tag events not fulfilling first layer criteria.

125 to shower axis is detected. The distribution of this variable for different particle  
 126 species is shown in Fig. 6.

127 Before using the variables listed above as input to the BDT method, we check that  
 128 the variables distributions in the simulation are in agreement with data for the muon and  
 129 electron beams which are quite pure. Figures 1 - 6 show that there is globally a good  
 130 agreement for the six variables of the two species even though the agreement is not perfect  
 131 in particular for electrons.

### 132 3.2 The two approaches to build the BDT-based classifier

133 In order to take into account the small difference observed in some variable distributions  
 134 between data and simulation, and to cross-check the particle identification using the BDT  
 135 method, we adopt two different training strategies for the BDT-based classifier. The first  
 136 approach, referred to as MC Training, uses simulation samples of pions, electrons and  
 137 muons as training sets. The second, referred to as Data Training, uses simulation samples  
 138 of pions but electron and muon samples taken from data as training sets.

#### 139 3.2.1 MC Training Approach

140 The six variables of the simulated pion, muon and electron events described in section  
 141 3.1 are used for the training and testing of the classifier. Events are chosen in alternating  
 142 turns for the training and test samples as they occur in the source trees until the desired  
 143 numbers of training and test events are selected. The training and test samples contain  
 144 the same number of events for each event class. Independent samples of signal events



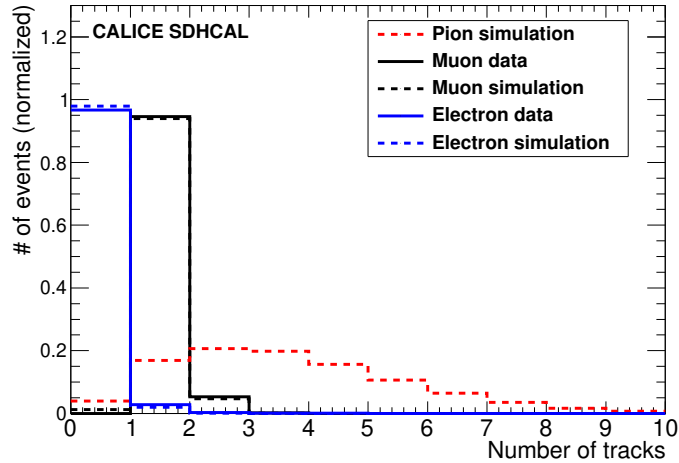


**Figure 2.** Distribution of number of the tracks in the shower (TrackMultiplicity). Continuous lines refer to data while dashed ones to the simulation.

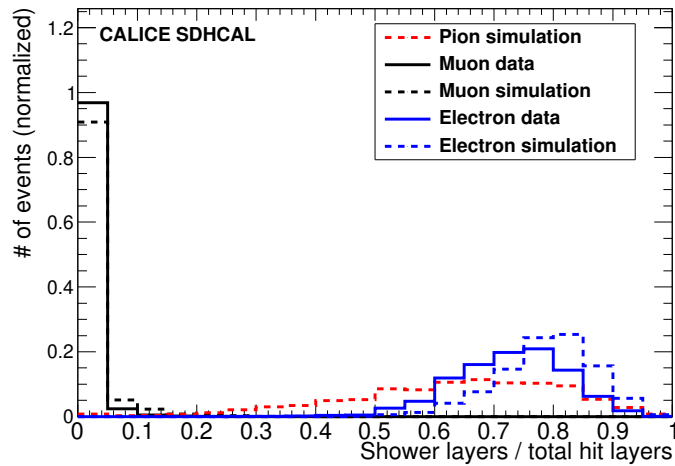


**Figure 3.** Distribution of ratio of the number of layers in which RMS of the hits' position in the  $x$ - $y$  plane exceeds 5 cm over the total number of fired layers ( $N_{\text{interactingLayers}}/N_{\text{Layers}}$ ). Continuous lines refer to data while dashed ones to the simulation.

145 (pions) and of the different background contributions (electron and muons) are used. The  
 146 ratio between signal and each background (electron or muon) events is 1 for training and  
 147 test samples. After the training, the BDT provides the relative weight of each variable  
 148 as a measure of distinguishing signal from background. Two BDT-based classifiers are  
 149 proposed here. The first ( $\text{BDT}_{\pi\mu}$ ) is used to discriminate pions against muons and the  
 150 second ( $\text{BDT}_{\pi e}$ ) to discriminate against electrons. Table 1 shows the variable ranking  
 151 according to their separation power in the  $\text{BDT}_{\pi\mu}$  while Tab. 2 gives their separation power

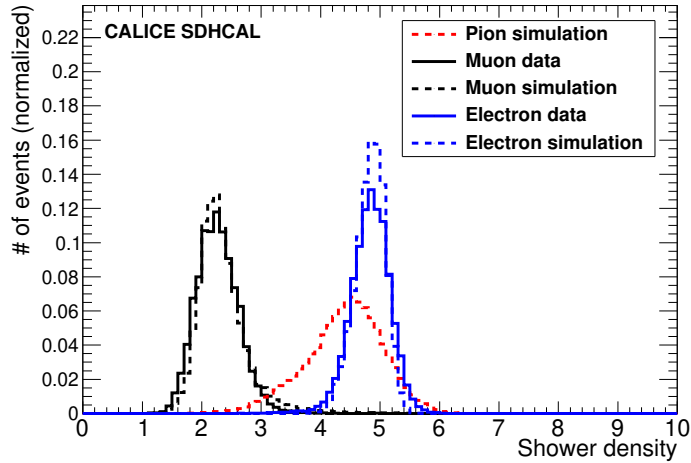


**Figure 4.** Distribution of the average number of neighbouring hits surrounding one hit (Density). Continuous lines refer to data while dashed ones to the simulation.

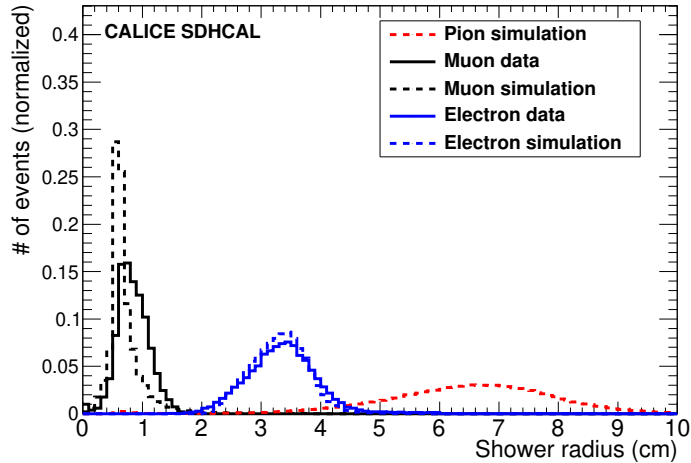


**Figure 5.** Distribution of the average radius of the shower (Radius). Continuous lines refer to data while dashed ones to the simulation.

152 in the case of  $BDT_{\pi e}$ . The BDT algorithm using the variables and their respective weights  
 153 is then applied to the test samples. The output of the BDT applied to each of the test sample  
 154 events is a variable belonging to the interval  $[-1,1]$  with the positive value representing  
 155 more signal-like events and the negative more background-like events.

156 Figure 7 (left) shows the output of the BDT for a test sample made of pions and  
 157 muons while Fig. 7 (right) shows the output for a test sample made of pions and elec-  
 158 trons. The values differ significantly for signal and background suggesting thus a large  
 159 separation power of the BDT approach. This is confirmed by Fig. 8. The pion selection

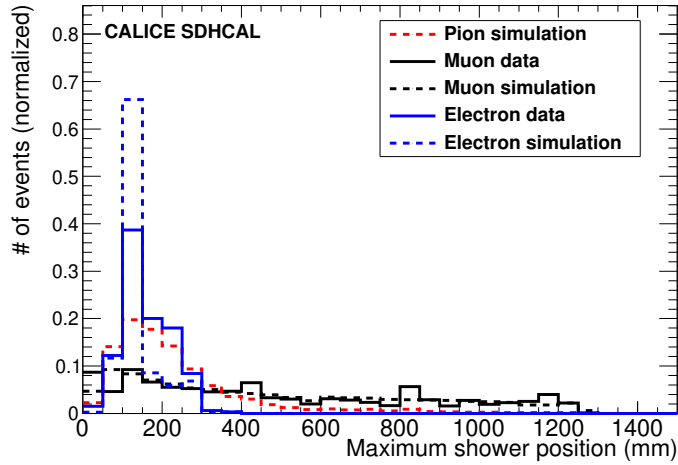


**Figure 6.** Distribution of the position of the layer with the maximum radius (Length). Continuous lines refer to data while dashed ones to the simulation.

**Table 1.** Variable ranking of separation power in the case of  $BDT_{\pi\mu}$ .

Rank : Variable	Variable relative weight
1 : Length	0.233
2 : Density	0.225
3 : NInteractinglayer/Nlayer	0.163
4 : Radius	0.160
5 : Begin	0.139
6 : TrackMultiplicity	0.080

**Table 2.** Variable ranking of separation power in the case of  $BDT_{\pi e}$ .

Rank : Variable	Variable relative weight
1 : Radius	0.204
2 : NInteractinglayer/Nlayer	0.203
3 : Density	0.194
4 : Length	0.151
5 : Begin	0.145
6 : TrackMultiplicity	0.101

160 efficiency versus the muon (electron) rejection of the test sample is shown in Fig. 9 (left)  
 161 and Fig. 9 (right), respectively. A pion selection efficiency exceeding 99% with a muon  
 162 and electron rejection of the same level ( $> 99\%$ ) can be achieved.

163 In order to check the validity of these two classifiers, we use the pure beam samples of

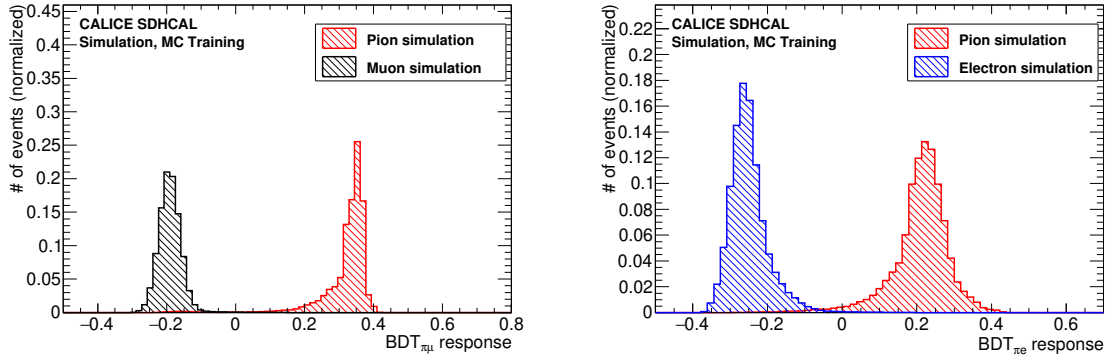


**Figure 7.** The BDT output of the  $\text{BDT}_{\pi\mu}$  (left) and  $\text{BDT}_{\pi e}$  (right) built with simulation samples.

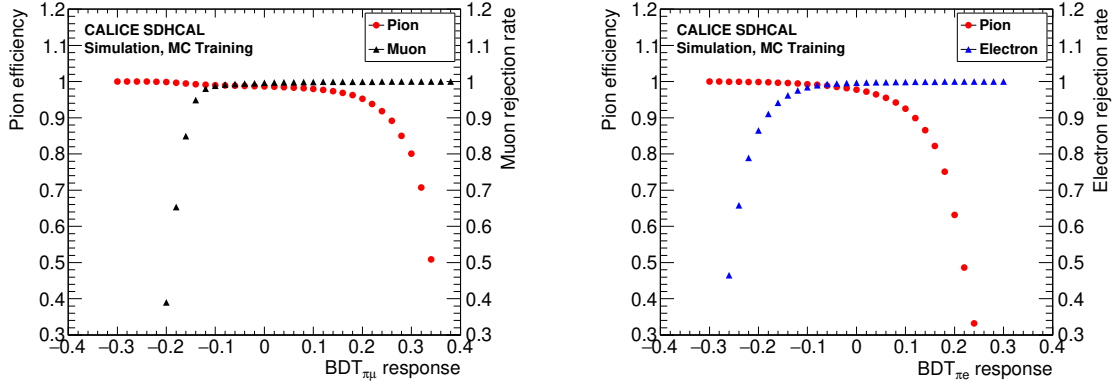


**Figure 8.** Pion efficiency and muon rejection rate (left) and pion efficiency and electron rejection rate (right) as a function of the BDT output.

164 muons and electrons. Figure 10 (left) shows the BDT output of  $\text{BDT}_{\pi\mu}$  and Fig. 10 (right)  
 165 shows the case of  $\text{BDT}_{\pi e}$ . Beam muon results show a good agreement with respect to the  
 166 simulated events. A slight shift of the beam electron shape is observed with respect to the  
 167 one obtained from the simulated events. This difference is most probably due to the fact  
 168 that the distribution of some variables in data and in the simulation are not identical. Next,  
 169 as a first step of purifying the collected hadronic data events we apply the pion-muon  
 170 classifier. Figure 10 (left) shows the  $\text{BDT}_{\pi\mu}$  response applied to the collected hadron  
 171 events in the SDHCAL. We can clearly see that there are two maxima. One maximum in  
 172 the muon range corresponds to the muon contamination of pion data and another one in the  
 173 pion range. Hence, to ensure the rejection of the muons in the sample, the BDT variable is  
 174 required to be  $> 0.1$ . The second step is to apply the  $\text{BDT}_{\pi e}$  to the remaining of the pion  
 175 sample. Figure 10 (right) shows the  $\text{BDT}_{\pi e}$  output. In order to eliminate the maximum  
 176 of the electrons contamination and get almost a pure ( $> 99.5\%$ ) pion sample with limited  
 177 loss of pion events, we apply to the pion samples a  $\text{BDT}_{\pi e}$  cut of 0.05.

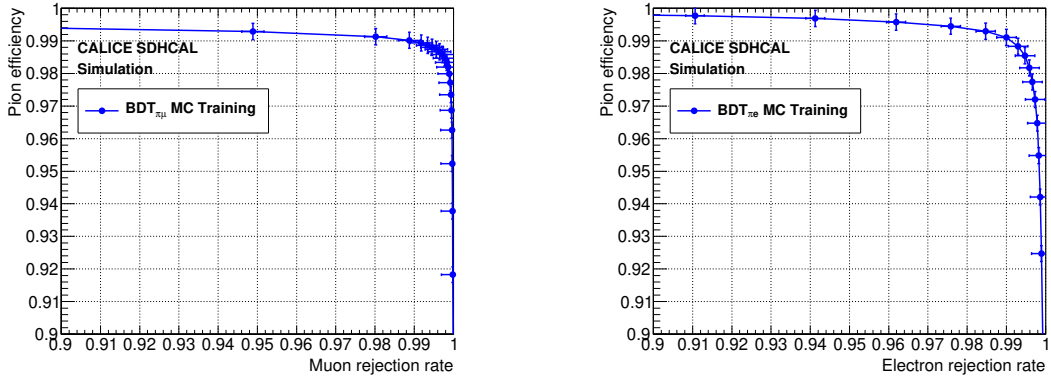


**Figure 9.** Pion efficiency versus muon rejection rate(left) and pion efficiency versus electron rejection rate (right).

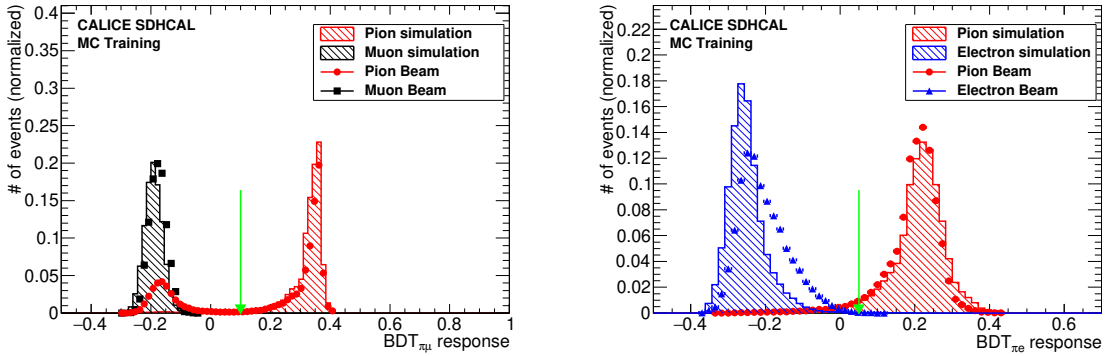


**Figure 10.** The BDT output after using the  $BDT_{\pi\mu}$  on the data pion sample (left) and the BDT output after using the  $BDT_{\pi e}$  on the same data pion sample after classified by  $BDT_{\pi\mu}$  (right). A green arrow is shown on both to indicate the BDT cut applied to clean the pion samples.

### 178 3.2.2 Data Training Approach

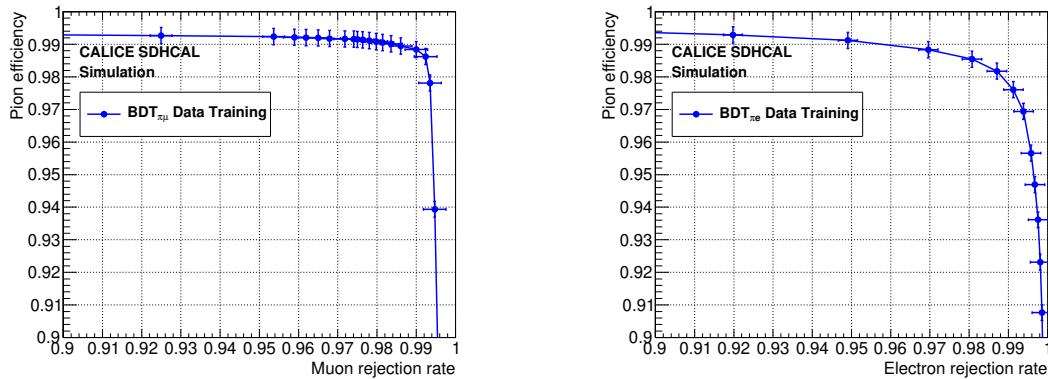
179 We use the same variables of the MC Training approach on the data samples of muons and  
 180 electrons but still on the simulated pion samples to build two classifiers. Then we apply  
 181 the same procedure as the MC Training approach. Table 3 and 4 show the corresponding  
 182 variables ranking for  $BDT_{\pi\mu}$  and  $BDT_{\pi e}$  according to their power separation importance.  
 183 The difference of variables weights of these two tables with respect to those obtained with  
 184 MC training approach is explained by the slight difference of some variables distributions  
 185 between data and simulation. Figure 11 left (right) gives the results of pion efficiency  
 186 and muon (electron) rejection rate. This shows that these two classifiers have very good  
 187 pion efficiency and high background rejection rate. The left (right) plot of Fig. 12 shows  
 188 the BDT output of the  $BDT_{\pi\mu}$  ( $BDT_{\pi e}$ ). Clearly these two classifiers have very good  
 189 separation power. We apply these classifiers to the raw pion beam samples. The results

**Table 3.** Variable ranking of separation importance in the case of  $\text{BDT}_{\pi\mu}$ .

Rank : Variable	Variable relative weight
1 : Length	0.300
2 : Radius	0.230
3 : Density	0.227
4 : Begin	0.103
5 : NInteractinglayer/Nlayer	0.080
6 : TrackMultiplicity	0.060

**Table 4.** Variable ranking of separation importance in the case of  $\text{BDT}_{\pi e}$ .

Rank : Variable	Variable relative weight
1 : Radius	0.195
2 : NInteractinglayer/Nlayer	0.191
3 : Density	0.189
4 : Length	0.151
5 : Begin	0.141
6 : TrackMultiplicity	0.131

**Figure 11.** Pion efficiency versus muon rejection rate (left) and pion efficiency versus electron rejection rate (right).

190 can be seen in Fig. 13. We apply a BDT cut value of 0.2 in the pion-muon separation stage  
 191 and then a BDT cut value of 0.05 in the pion-electron separation stage.

## 192 4. Results

193 The distributions of input variables for the data and simulation events of pion, muon and  
 194 electron are shown in Fig. 14. Only the pion data sample distributions are obtained after

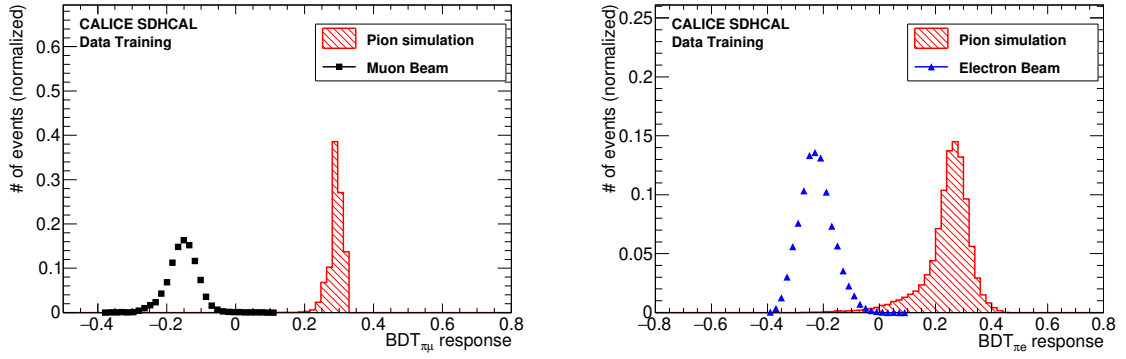


**Figure 12.** BDT output of the  $\text{BDT}_{\pi\mu}$  built with pure beam muons and simulated pion samples (left) and of the  $\text{BDT}_{\pi e}$  built with pure beam electrons and simulated pion samples (right)

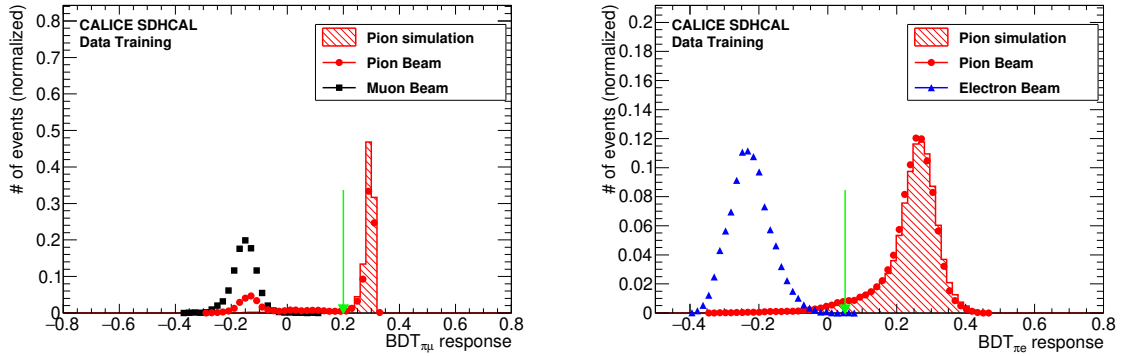


**Figure 13.** The BDT output after using the  $\text{BDT}_{\pi\mu}$  on the data pion sample (left) and the BDT output after using the  $\text{BDT}_{\pi e}$  on the same pion sample after classified by  $\text{BDT}_{\pi\mu}$  (right). A green arrow is shown on both to indicate the BDT cut applied to clean the pion samples.

195 applying the data-based BDT classifiers. A good agreement between the data and simu-  
 196 lation events for pions is observed. It also confirms the power of the BDT method. The  
 197 rejection of muons and electrons presented in the pion data sample using the BDT allows  
 198 us to have more statistics and a rather pure pion sample as explained in the previous sec-  
 199 tion. Figure 15 shows the results of comparison in event selection between the standard  
 200 method and the BDT-based method using the simulation samples. For both simulation and  
 201 beam data, the BDT method leads to more statistics comparing to the standard method [7]  
 202 in particular at low energy as shown in Fig. 16 for the comparison of the selected events  
 203 as a function of the total number of hits for the 10 GeV pion beam data. We also do not  
 204 observe any significant deviation of energy resolution when applying the standard energy  
 205 reconstruction described in Ref. [7] on the pion events selected by the BDT method.

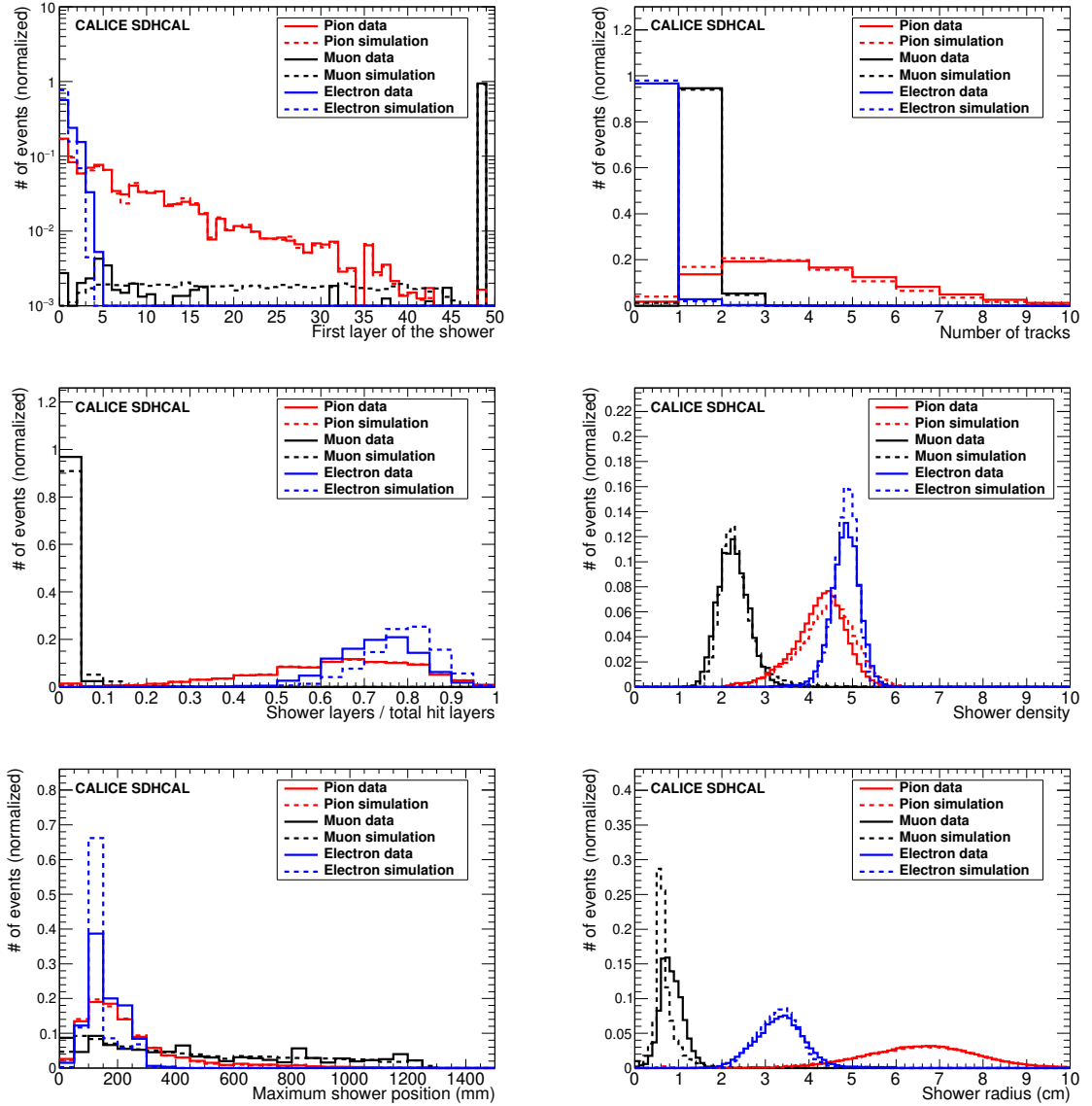


**Figure 14.** Distributions of six input variables of electron, muon and pion samples. Continuous lines refer to data and dashed ones to the simulation. The pion samples are classified with the data-based training BDT method and others is obtained without applying BDT-based classifiers.

## 206 5. Conclusion

207 A new particle identification method using BDT-based MVA technique is applied to purify  
 208 the pion events collected at the SPS H2 beamline in 2015 by the CALICE SDHCAL proto-  
 209 type. The new method uses the topological shape of events associated to muons, electrons  
 210 and pions in the CALICE SDHCAL to reject the two first species. A significant statis-  
 211 tical gain is obtained with respect to the standard method used in the work presented in  
 212 Ref [7]. This statistical gain is particularly significant at energies up to 40 GeV and can be



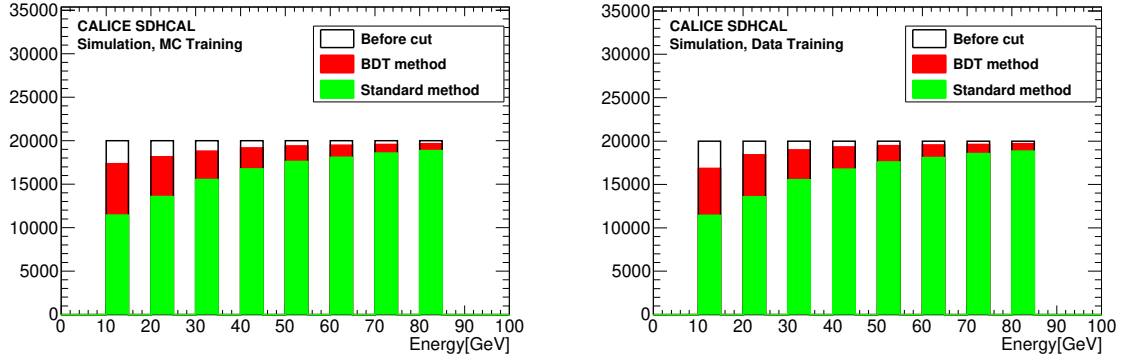


**Figure 15.** The number of simulated events of different energy points from 10 GeV to 80 GeV before (white) and after applying the standard method (green) or BDT method (red). The left plot shows the results from BDT method with MC Training approach while the right one shows the results with Data Training approach.

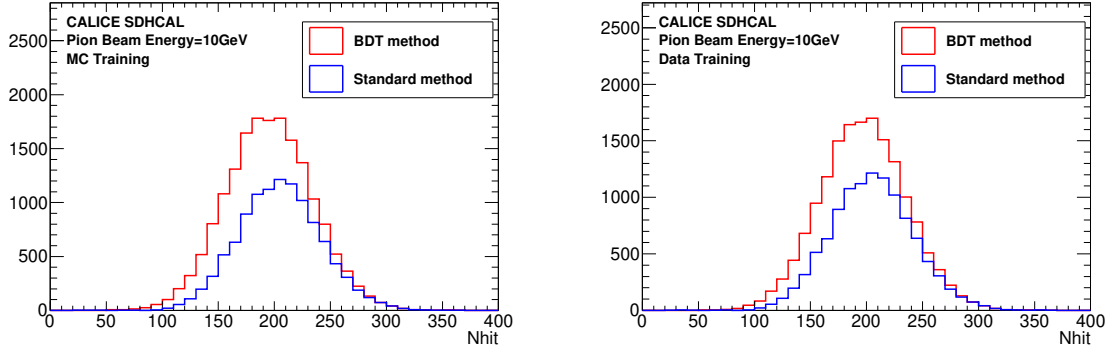


**Figure 16.** Distribution of the total number of hits for the 10 GeV pion beam data selected by the standard method (blue) and the BDT method (red). The left plot shows the results from BDT method with MC Training approach while the right one shows the results with Data Training approach.

213 explained by the fact that the showers that start in the first layers are not all rejected. This  
 214 gain shows the better efficiency and separation power of the multivariate approach over  
 215 the cut-based approach of the standard method. The BDT-based particle identification in  
 216 CALICE SDHCAL is a robust and a reliable method as confirmed by the results of two  
 217 different training approaches.

## 218 6. Acknowledgements

219 This study was supported by National Key Programme for S&T Research and Develop-  
 220 ment (Grant NO. 2016YFA0400400).

## 221 **References**

- 222 [1] G. Baulieu et al., Construction and commissioning of a technological prototype of a  
223 high-granularity semi-digital hadronic calorimeter, *JINST* **10** (2015) P10039.
- 224 [2] T. Abe et al., The International Large Detector: Letter of Intent, FERMILAB-LOI-2010-01,  
225 FERMILAB-PUB-09-682-E, DESY-2009-87,  
226 KEK-REPORT-2009-6, (2010) arXiv:1006.3396.
- 227 [3] M. A. Thomson, Particle Flow Calorimetry and the PandoraPFA Algorithm, *NIMA* **611 25**  
228 (2009), arXiv:0907.3577
- 229 [4] V. L. Morgunov, Calorimetry design with energy-flow concept (imaging detector for  
230 high-energy physics), in Proc of Int. Conf. on Calorimetry (Calor02), (2002) Pasadena, 70
- 231 [5] J. C. Brient and H. Videau, The calorimetry at the future e+e- linear collider, in Proc. of  
232 APS/DPF/DBP summer study on the future of particle physics, (2002) Snowmass, Colorado  
233 [hep-ex/0202004]
- 234 [6] F. Dulucq, C. de la Taille, G. Martin-Chassard, N. Seguin-Moreau, HARDROC: Readout  
235 chip for CALICE/EUDET Digital Hadronic Calorimeter, IEEE Nuclear Science Symposium  
236 & Medical Imaging Conference, IEEE, 2010.
- 237 [7] CALICE collaboration, First results of the CALICE SDHCAL technological prototype,  
238 *JINST* **11** (2016) P04001.
- 239 [8] B. P. Roe, H. J. Yang, J. Zhu et al., Boosted decision trees as an alternative to artificial neural  
240 networks for particle identification, *NIMA* **543** (2004) 577-584.
- 241 [9] H. J. Yang, B. P. Roe, J. Zhu et al., Studies of boosted decision trees for MiniBooNE particle  
242 identification, *NIMA* **555** (2005) 370-385.
- 243 [10] A. Hoecker, P. Speckmayer, J. Stelzer, J. Therhaag, E. von Toerne and H. Voss,  
244 TMVA-Toolkit for multi data analysis, arXiv:physics/0703039.
- 245 [11] S. Agostinelli et al. GEANT4 - a simulation toolkit, *NIMA* **506** (2003) 250-303.
- 246 [12] V. V. Uzhinsky, The Fritiof (FTF) Model in Geant4, 2013.
- 247 [13] G. Folger, V. N. Ivanchenko, et J. P. Wellisch, The binary cascade. *The European Physical*  
248 *Journal A-Hadrons and Nuclei*, 2004, vol. 21, no 3, p. 407-417.
- 249 [14] Z. Deng et al., Tracking within Hadronic Showers in the CALICE SDHCAL prototype using  
250 a Hough Transform Technique, *JINST* **12** (2017) P05009-P05009.
- 251 [15] CALICE collaboration, Resistive Plate Chamber Digitization in a Hadronic Shower  
252 Environment, *JINST* **11** (2016) P06014, arXiv:1604.04550.